

SLAT BROADBAND NOISE PREDICTION OF MULTI-ELEMENT 30P30N AIRFOIL BY A HYBRID RANS-LES METHOD

Tongrui Peng⁽¹⁾, Yufeng Yao⁽²⁾, and Quanmin Zhu⁽³⁾

*⁽¹⁾ Engineering Modelling and Simulation Research Group, University of the West of England, U.K.,
 Email: tongrui2.peng@live.uwe.ac.uk*

*⁽²⁾ Engineering Modelling and Simulation Research Group, University of the West of England, U.K.,
 Email: Yufeng.Yao@uwe.ac.uk*

*⁽³⁾ Engineering Modelling and Simulation Research Group, University of the West of England, U.K.,
 Email: Quan.Zhu@uwe.ac.uk*

ABSTRACT

This paper presents a combined CFD and CAA study to assess the slat noise emissions from a multi-element 30P30N airfoil at the 5-degree and 8-degree angle of attack, using a hybrid RANS-LES method. In this simulation, the structured mesh is used and steady-state convergence criterion is 1×10^{-3} . The inflow Mach number is 0.17, and Reynolds number based on inflow velocity and the chord length of the airfoil is 1.8×10^6 . It has been found that the surface static pressure coefficient distributions at both angles are in good agreement with the experiments and the predicted lift coefficients are close to the measurements calculated from steady RANS. The mean vertical velocity of unsteady flow is well compared with measurement results while some difference existing for mean streamwise velocity. Finally, the steady-state broadband noise distribution shows that slat leading edge and trailing edge are two main noise sources of slat noise.

1. INTRODUCTION

With the advent of quieter, ultra-high-bypass-ratio engines, airframe noise is becoming an important contributor to aircraft noise during approach [1]. Both model-scale tests and flyover noise measurements have shown that the leading-edge slat is a prominent source of airframe noise during approach conditions. Slat noise consists of two components, a high-frequency tonal noise signature and a broadband noise spectrum covering the lower and mid frequencies [2]. Based on

experimental results, slat tonal noises emit from the region in the vicinity of slat trailing edge while slat broadband noise originates from unsteady flow in the slat cove part [2]. For tonal noises prediction, several researchers have already done [3,4].

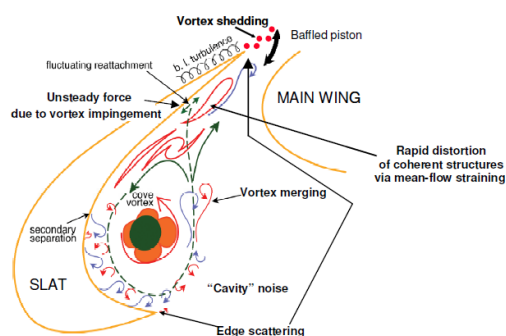


Figure 1. Potential sources and physical mechanisms behind noise generation near a leading edge slat [5]

Slat noise is a complex aeroacoustic problem consisting of the different physical mechanism. (Fig. 1) and for slat noise prediction, Pagani et al (2017) used a closed-section, closed wind tunnel to predict slat broadband noise. The angle of attacks range from 2-degree to 10-degree and freestream velocity ranges from 24 m/s to 34m/s [6]. The results show that broadband noise is well characterized for Strouhal numbers between 5 and 20 [6].

In 2018, Li et al used D5 aeroacoustic wind tunnel at Beihang University to predict slat noise [7]. The surface static pressure distributions measured in D5 are similar to the results from Japan Aerospace Exploration Agency (JAXA) wind tunnel test [8], verifying the similarity of the low field and the reliability of experiments. For acoustic field, noise spectral shape, tonal frequency, and noise source location all agree well with earlier investigations and numerical simulations [7]. Apart from experimental methods for slat noise prediction, currently, most studies choose CFD (Computational Fluid Dynamics) combined with the acoustic analogy method as the primary choice for slat noise prediction. However, the complicated physical mechanism at slat cove part makes traditional RANS method hard to accurately predict slat noise. Therefore, a new method called hybrid RANS/LES has gradually been widely used [9,10,11]. For the present study, acoustic data is the fundamental part of future noise cancellation. Therefore, the objective of the present study is aimed at predicting accurately the noise from a 30P30N high-lift configuration with DES *SST k- ω* method.

This paper is organized as follows: Section 2 describes numerical method used; Section 3 describes the problem and how to carry out computation; Section 4 provides results of static surface pressure coefficient, unsteady mean velocity, vorticity and instantaneous vorticity; Section 5 describes acoustic prediction results from ANSYS broadband noise model; Section 6 concludes main achievements and future work.

2. NUMERICAL METHODS

2.1. Flow solver

Currently, available prediction methods are the fully analytic method, CFD (Computational Fluid Dynamics) combined with the acoustic analogy method, the semi-empirical method, and fully numerical method [7].

In this study, the commercial Computational Fluid Dynamics (CFD) was employed to compute flow field and the main CFD tool is ANSYS Fluent software, the most widely used powerful CFD tool.

2.2. Turbulence model

The two-equation Shear Stress Transport (*SST k- ω*) model is used for presented problems, as the *k- ω* model of turbulence is capable of solving turbulence parameters very close to boundary or wall region. Besides, *SST k- ω* turbulence model often has good behavior in adverse pressure gradients and separating flow [12].

For steady flow simulation, steady RANS *SST k- ω* is the ideal choice and hybrid RANS/LES method like Detached Eddy Simulation (DES) *SST k- ω* is selected as

the preferred model for unsteady flow simulation. For acoustic field, ANSYS broadband noise model is used to highlight noise sources at slat cove part under steady-state condition.

The spatial terms are discretized by using the second-order upwind scheme to make sure high order accuracy. The pressure-velocity coupling is dealt with the COUPLED algorithm.

3. PROBLEM DEFINITION AND COMPUTATIONAL PROCEDURE

Currently, the most popular object used for slat noise prediction is MD 30P30N (Fig. 2), designed by McDonnell-Douglas (now Boeing), corresponds to slat and flap deflections of 30° each is selected as the object [8]. The chord length c is 0.457 m while slat chord length is 15% of the chord length.



Figure 2. MD 30P30N [7]

In this simulation, MD 30P30N is used for slat broadband noise prediction and C-domain type is used for generating meshes in ICEM software. The radius for C-domain is $65.6c$ while both upper and lower lengths are same. For wake region, the length is $65.6c$. Topology can be seen in Fig. 3. There are totally 64 blocks in C-domain, and Fig. 4 displays the mesh.

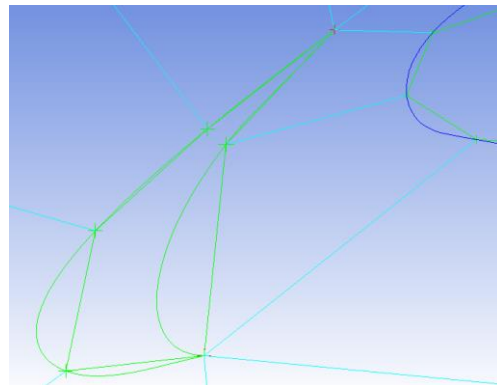


Figure 3. Topology for slat foil

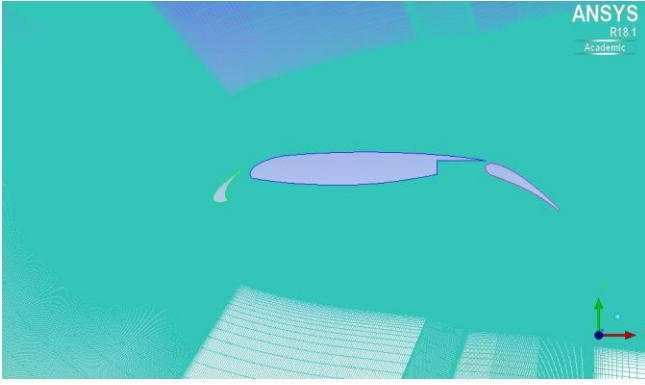


Figure 4. Mesh

Tab. 1 has core information about these two meshes.

Table 1. Mesh Parameters Summary

Name	Mesh 1	Mesh 2
Total number of grids	1,181,670	2,086,611
Grids at slat cove part	21,000	170,522
y^+	1	1
Points around slat foil	400	729

Tab. 2 has several flow parameters needed in Fluent software. Reynolds number based on stowed chord length is 1.8 million and y^+ value equals to 1. Convergence criterion for steady RANS is 1×10^{-3} and turbulence intensity for inlet is 4.5%.

Table 2. Flow Properties

Parameter	Value
Mach Number	0.17
Reynolds Number	1.8e6
Chord length, c	0.457
Chord length for slat, c_s	0.0685
Freestream velocity, U_∞	57.8
Temperature, T	289
Dynamic Viscosity, μ	1.79e-5

Time step size in this simulation is 7.19×10^{-4} , calculated from Strouhal number 5 [6] and 20 time steps. For each unsteady simulation, to lower the effects of initial transient state on both mean flow and statistical quantities, the first 7000 time steps were discarded and typically, 10,000 time steps were used to performing average and extract turbulent statistics as there is no significant deviations in mean velocity distribution noted for longer time records [15].

4. RESULTS AND DISCUSSION

4.1. Steady flow prediction

For validation purpose, it is better and convenient to start with a comparison of mean pressure distribution along the surface of each element of the high-lift system. The steady RANS *SST k- ω* was used for obtaining surface static pressure coefficient C_p distribution for 5-degree AOA and 8-degree AOA. These values were essential equals to those based on the time average of the unsteady solutions [15].

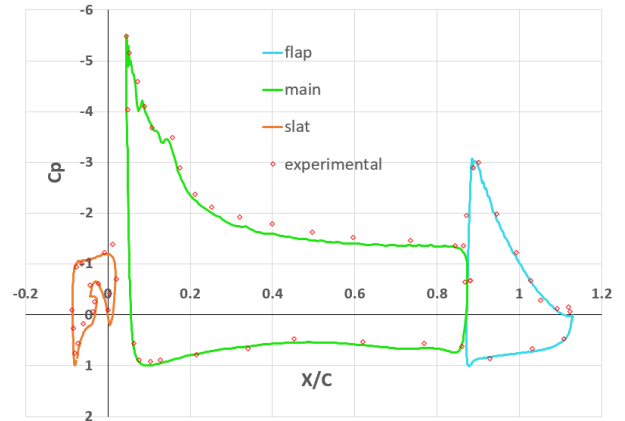


Figure 5. Surface pressure distribution at Mach=0.17 and AOA=5 degrees

Fig. 5 displays C_p distributions on all three elements at 5-degree AOA. Note that maximum value of the ordinate for each element part is different. Overall, good agreement is observed between JAXA experimental results and Computational Fluid Dynamics (CFD) simulated results. The accurately C_p predictions at main foils leading edge provide some confidence that flow at slat gap part might be properly captured as slat foil is the crucial aim of this simulation part. Meanwhile, the prediction at flap foil is also well. The notable difference from main foil upper surface that ordinate value of experimental results are slightly higher than computational results between $x/c=0.2$ and $x/c=0.7$ and the difference value is roughly 0.2.

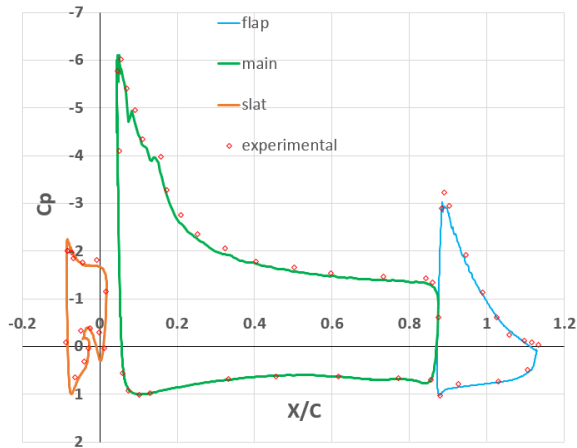


Figure 6. Surface pressure distribution at Mach=0.17 and AOA=8 degrees

Fig. 6 presents C_p distribution at an 8-degree AOA. At this angle, for flap foil, a noticeable underprediction of C_p between $x/c=0.83$ and $x/c=0.85$ can be observed in Fig. 6. Once again, however, there is a satisfactory agreement between experimental results and computed results for pressure along slat surface and main element surface for the 8-degree AOA case.

4.2. Unsteady flow prediction

The lift coefficient value for steady state flow simulation result is 2.90. Tab. 3 summarizes lift coefficient characteristics for unsteady flow simulation by averaging over nearly 10,000 time steps.

Table 3. Mathematical characteristics of lift coefficient

Maximum Value	2.905
Average Value	2.89
Minimum Value	2.87

It can clearly see that average lift coefficient C_l value for unsteady state flow simulation is close to lift coefficient C_l value for steady state flow simulation. Therefore, Detached Eddy Simulation (DES) can be a reliable method to predict lift coefficient.

Fig. 7 and Fig. 9 show the contour of mean streamwise (U) and vertical (V) velocity for 8-degree AOA, extracted from time-accurate simulations by averaging 10,000 time steps. Fig. 8 and Fig. 9 display the contour of streamwise and vertical velocity for 8-degree AOA from PIV measurements and computational results by using CFL3D code [15]. The ranges of velocity value in Fig.7 and Fig. 9 are scaled based on ranges from PIV measurements published by Khorrami et al [15].

The streamwise velocities at slat leading edge and trailing edge are accurately predicted by the

computations. See dark red contour in Fig. 7. Besides, high negative velocities at cove part can be observed. This is imposed by the recirculating flow field. Meanwhile, compare two computational results from Fig. 7 and Fig. 8, it is clear that for both simulation results, the notable difference between measured and predicted velocities occurs at slat leading edge part. The streamwise contour shows that significant positive velocities penetrate towards cove wall. However, a clear vortex exists near slat leading edge in Fig. 7. It might indicate that turbulent flow is not fully simulated here.

For mean vertical velocity, compared with PIV measurement results, the computed vertical velocity contour (Fig. 9) shows the proper acceleration at main foil leading edge and further into slat gap.

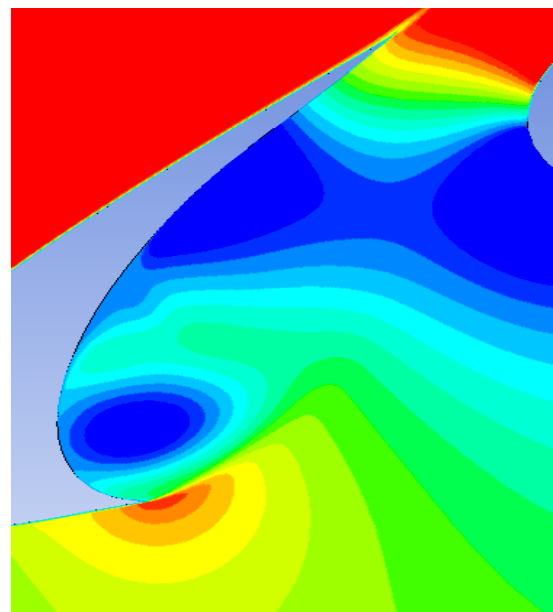


Figure 7. Mean streamwise velocity

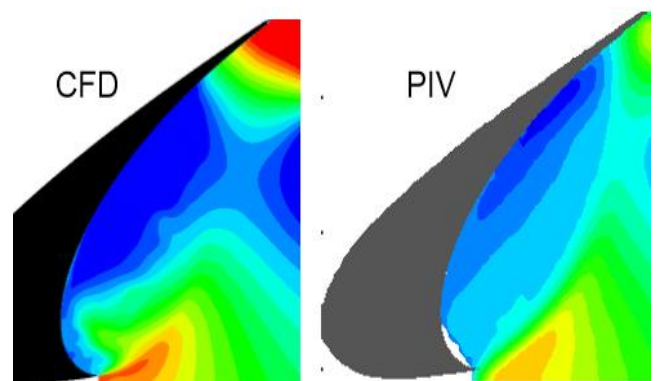


Figure 8. Averaged streamwise velocity field for 8-degree AOA from CFD and PIV [15]

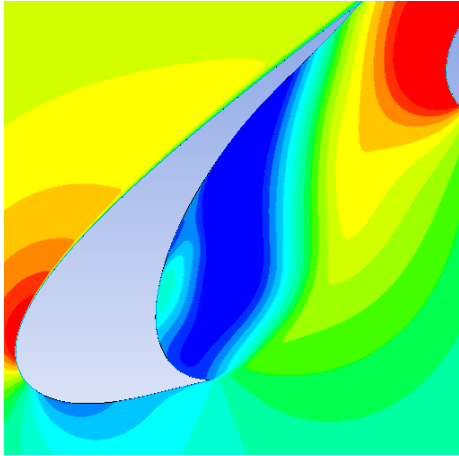


Figure 9. Mean vertical velocity

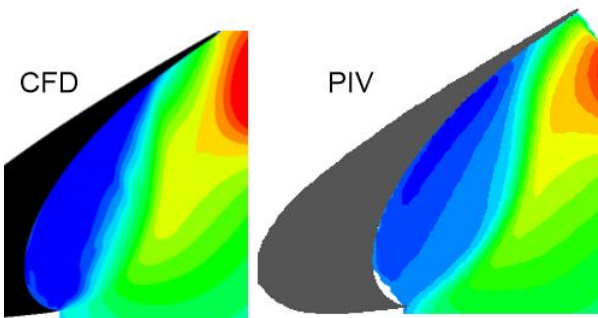


Figure 10. Averaged vertical velocity field for 8-degree AoA from CFD and PIV [15]

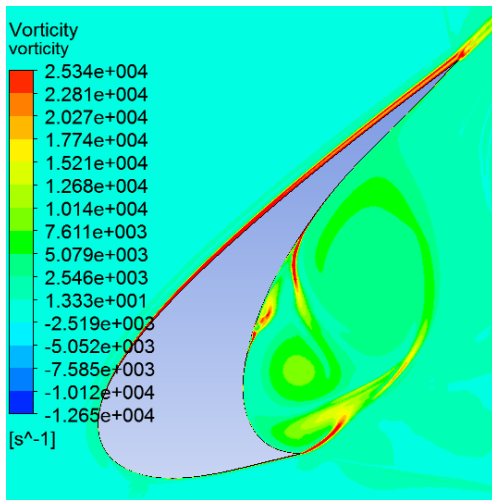


Figure 11. Vorticity magnitude

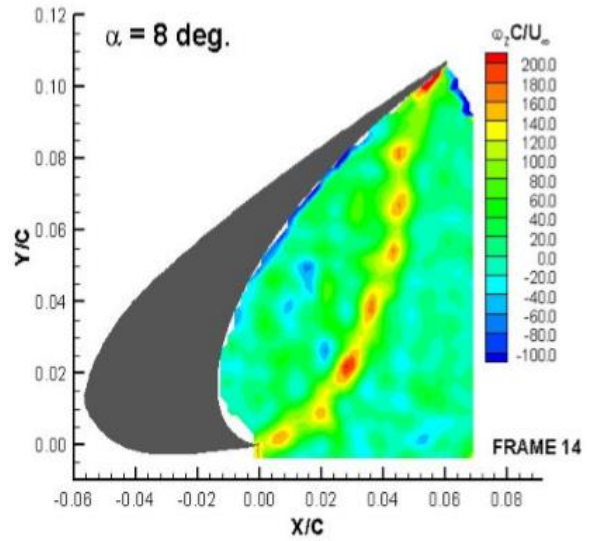


Figure 12. Measured Instantaneous vorticity field at 8-degree AoA [15]

The instantaneous vorticity plot from the 8-degree simulation is presented in Fig. 11, roughly corresponding to 9900 in the sampled record of 10,000 time steps. Fig. 12 shows the PIV measurement result captures individual vortices and their upward convection by the shear layer [15]. The maximum and minimum values of vorticity (Fig. 11) are scaled based on the corresponding value in Fig. 12. Compared with PIV results, vortex rolling-up is not seeing and the reattachment point is moving far away from slat trailing edge. For once-through flow, the time is 60 (the domain length) divide 57.8 (freestream velocity) and the value is roughly 1.04s. Simulation time for this unsteady flow is 12.223 seconds, which means during simulation time, 11 times through-flow had completed, and it indicates that time is enough. Therefore, the potential reason is for larger time step size.

In general, both mean and instantaneous PIV measurements indicate that pattern of vortex structure at slat cove part is more chaotic than simulated flow results.

5. ACOUSTIC FIELD PREDICTION

ANSYS broadband model has five different sub-models inside and it can enable users to quantify the local contribution to the total acoustic power generated by the steady-state flow. As physical mechanism at slat cove part is complex, therefore, it will be helpful to identify potential noise sources under steady-state condition.

Fig. 13 and Fig. 14 display acoustic power level for two angles. These computations obtained from steady RANS simulation. Acoustic power Levels are high at

slat leading edge and trailing edge for both 5-degree AOA and 8-degree AOA.

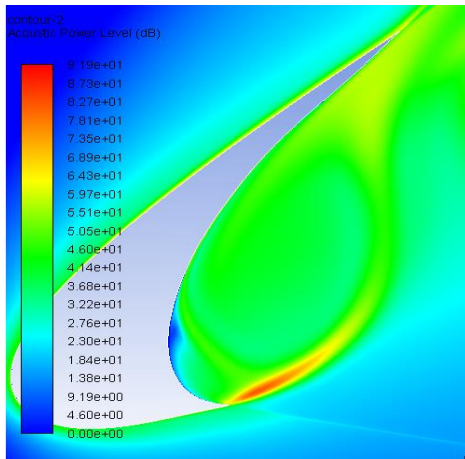


Figure 13. Broadband acoustic power level for AoA=5 degrees

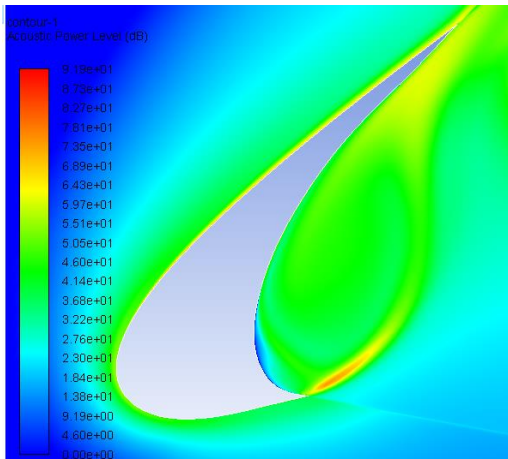


Figure 14. Broadband acoustic power level for AoA=8 degrees

6. CONCLUSION AND FUTURE WORK

A set of simulations has been conducted on the MD 30P30N high-lift three-element airfoil by using hybrid RANS/LES method on the structured mesh. The surface pressure coefficients C_p distribution computational results under steady RANS at both 5-degree and 8-degree agree well with JAXA wind tunnel. Unsteady state flow simulation using DES method at 8-degree AOA show that mean vertical velocity agree well with PIV results and notable differences can be observed for mean streamwise velocity. Besides, for instantaneous vorticity, vortex rolling-up can be captured and this might be due to larger time step size. This should be investigated in further to capture individual vorticity. For acoustic field, acoustic power level through steady RANS and ANSYS Broadband Noise Model shows the

noise sources in slat cove part, provide convenient information for further noise prediction. Future work to obtain acoustic data is required. As acoustic data is the fundamental part of the entire noise cancellation project. Besides, after obtaining acoustic data, modern control method like U-model [16] will add to design the new controller to do noise cancellation.

7. ACKNOWLEDGMENTS

The first author gratefully acknowledges partial finance support from UWE Bristol for attending this conference.

8. REFERENCES

- Choudhari, M., Lockard, D., Khorrami, M. & Mineck, R. (2011). Slat noise simulations: Status and challenges. 40th International Congress and Exposition on Noise Control Engineering 2011, INTER-NOISE. pp. 361-368.
- Agarwal, A. & Morris, P. (2006). Prediction Method for Broadband Noise from Unsteady Flow in a Slat Cove. *AIAA Journal*. 44(2), pp. 301-310.
- Khorrami, M.R., Singer, B.A. & Berkman, M.E. (2002). Time-Accurate Simulations and Acoustic Analysis of Slat Free Shear Layer. *AIAA Journal*. 40(7), pp. 1284-1291.
- Agarwal, A. & Morris, P. (2002). Investigation of the Physical Mechanisms of Tonal Sound Generation by Slats, AIAA Paper. 2002-2575.
- Choudhari, M. & Lockard, D. (2015). Assessment of Slat Noise Predictions for 30P30N High-Lift Configuration from BANC-III Workshop, 21st AIAA/CEAS Aeroacoustics Conference, AIAA Paper. 2015-2844.
- Pagani, C.C., Souza, D.S. & Medeiros, M.A.F. (2017). Experimental investigation on the effect of slat geometrical configurations on aerodynamic noise. *Journal of Sound and Vibration*. 394, pp. 256-279.
- Li, L., Liu, P., Guo, H., Geng, X., Hou, Y. & Wang, J. (2018). Aerodynamic and aeroacoustics experimental investigation of 30P30N High-lift configuration. *Applied Acoustics*. 132, pp. 43-48.
- Murayama, M., Nakakita, K., Yamamoto, K., Ura, K., Ito, Y. & Choudhari, M.M. (2014). Experimental Study on Slat Noise from 30P30N Three-Element High-Lift Airfoil at JAXA Hard-Wall Low-speed Wind Tunnel, 20th AIAA/CEAS Aeroacoustics Conference, AIAA Paper. 2014-2080.

9. Ashton, N., West, A. & Mendonca, F. (2015). Slat Noise Prediction using Hybrid RANS-LES methods on Structured and Unstructured Grids, 21st AIAA/CEAS Aeroacoustics Conference, AIAA Paper. 2015-3139.
10. Terracol, M. (2006). A zonal RANS/LES approach for noise sources prediction. *Flow Turbulence and Combustion* 77(1), pp. 161-184.
11. Nebenfuhr, B., Yao, H., Peng, S. & Davidson, L. (2013). Hybrid RANS/LES Simulations for Aerodynamic and Aeroacoustic Analysis of a Multi-Element Airfoil, 19th AIAA/CEAS Aeroacoustics Conference, AIAA Paper. 2013-2066.
12. Menter, F. R. (1993). Zonal Two Equation $k-\omega$ Turbulence Models for Aerodynamic Flows, AIAA Paper. 1993-2906.
13. Gao, J., Li, X. & Li, D. (2017). The Effect of slat trailing edge thickness on the noise from a 30p30n highlift configuration. 24th International Congress on Sound and Vibration. London, 23-27 July 2017.
14. Jenkins, L.N., Khorrami, R.M. & Choudhari, M.M. (2004). Characterization of Unsteady Flow Structures Near Leading-Edge Slat: Part I. PIV Measurements, 10th AIAA/CEAS Aeroacoustics Conference, AIAA Paper. 2004-2801.
15. Khorrami, M.R., Choudhari, M.M. & Jenkins, L.N. (2004). Characterization of Unsteady Flow Structures Near Leading-Edge Slat: Part II. 2D Computations, 10th AIAA/CEAS Aeroacoustics Conference, AIAA Paper. 2004-2801.
16. Zhu, Q., Yu, D. & Zhao, D. (2017). An enhanced linear Kalman filter (EnLKF) algorithm for parameter estimation of nonlinear rational models. *International Journal of Systems Science*. 48 (3), pp. 451-461.